# Hybrid Simulations of Plasma Transport by Kelvin-Helmholtz Instability at the Magnetopause: Density Variations and Magnetic Shear

M. M. Cowee, D. Winske, S. P. Gary

Los Alamos National Laboratory

M. M. Cowee, Los Alamos National Laboratory, Los Alamos, NM, 87544, USA. (mcowee@lanl.gov)

**Abstract.** Two-dimensional hybrid (kinetic ions, massless fluid electrons) simulations of the Kelvin Helmholtz Instability (KHI) for a magnetopause configuration with a varying density jump and magnetic shear across the boundary are carried out to examine how the transport of magnetosheath plasma into the magnetosphere is affected by these conditions. Low magnetic shear conditions where the magnetosheath magnetic field is within 30° of northward is included in the simulations because KHI is thought to be important for plasma transport only for northward or near-northward interplanetary magnetic field orientations. The simulations show that coherent vortices can grow for these near-northward angles, and that they are sometimes more coherent than for pure northward conditions because the turbulence which breaks-down these vortices is reduced when there are magnetic tension forces. With increasing magnetic shear angle and increasing density jump, the growth rate is reduced, and the vortices do not grow to as large of size which reduces the plasma transport. By tracking the individual particle motions diffusion coefficients can be obtained for the system, where the diffusion is not classical in nature but instead has a time dependence resulting from both the increasingly large-scale vortex motion and the small-scale turbulence generated in the break-down of the instabilities. Results indicate that diffusion on the order of $10^9$ $m^2/s$ could possibly be generated by KHI on the flanks of the magnetosphere.

## 1. Introduction

It is not well understood how the low latitude boundary layer (LLBL) is populated during northward IMF conditions when reconnection at the dayside magnetopause is not favored. The primary candidate mechanisms for this plasma entry are thought to be double high-latitude reconnection, diffusion resulting from plasma waves and drift instabilities, and the Kelvin-Helmholtz instability [see review in *Scholer and Treumann*, 1997; *Phan et al.*, 2005]. Evidence for double high-latitude reconnection has been seen by spacecraft and ground-based observations [e.g., *Lavraud et al.*, 2006; *Imber et al.*, 2007; *Marcucci et al.*, 2008] and analysis of the waves at the magnetopause suggests that they may be only marginally capable of the necessary diffusivities for populating the LLBL [e.g., *Scholer and Treumann*, 1997]. The role of Kelvin-Helmholtz instability (KHI) was initially expected to be minor because KHI was thought to be a surface wave phenomena that was not widely unstable and was not capable of fast or efficient plasma transport [e.g., *Axford*, 1964], but recent simulation work and observations indicate that KHI may be more important than initially thought. This manuscript focuses on the KHI as a plasma transport mechanism for northward IMF.

MHD and Hall-MHD simulations have shown that the instability is indeed unstable for a range of conditions at the magnetopause and that the instability grows beyond the surface wave to form rolled-up vortices which can engulf magnetosheath plasmas and transport them inside the magnetosphere as the vortex breaks down through reconnection or other process [e.g., *Huba*, 1994; *Min et al.*, 1997; *Nykyri and Otto*, 2001; *Nakamura and Fujimoto*, 2005; *Nykyri and Otto*, 2004]. Spacecraft have themselves seen evidence of

KH waves and rolled-up vortices on the flanks of the magnetosphere [e.g., *Ogilvie and Fitzenreiter*, 1989; *Chen et al.*, 1993; *Fairfield et al.*, 2000; *Hasegawa et al.*, 2004, 2006; *Taylor et al.*, 2008], however observations have not been able to quantify the degree of plasma mixing that is occurring. In order to better understand how effective KHI may be at transporting plasma across the boundary, we carry out hybrid simulations with kinetic ions and massless fluid electrons, so that we may track the individual particle motions. Although both MHD computations and hybrid simulations well represent the growth of the instability, only hybrid simulations follow individual particle motions and permit quantification of the plasma mixing.

Some of the first hybrid simulations (kinetic ion, fluid electron) of KHI at the magnetopause for northward IMF conditions were carried out by *Terasawa et al.* [1992] and *Thomas and Winske* [1993]. *Terasawa et al.* [1992] simulated one wavelength of the dominant KH mode for varying velocity shear layer width in a uniform density plasma and found that plasma mixing occurred on a timescale faster than the roll-up time of the vortex, which is the mixing time predicted by MHD theory. By calculating the number of simulation cells containing a mix of magnetosheath and magnetosphere plasmas, they determined that the plasma mixing increased with a "$t^2$" dependence. As the vortex grows, the individual particles become efficiently mixed within the vortex structure over spatial scales larger than a Larmor radius, which is the mixing layer thickness predicted by MHD theory. *Thomas and Winske* [1993] used a larger simulation box to model the growth of several vortices and found that in this case the mixing does not follow a $t^2$ dependence but instead shows a more linear temporal dependence. When the simulation box is large enough to allow are multiple vortices, they coalesce together to form even

larger vortices until there is one final vortex of the size of the simulation box. Yet even though the plasma mixing did not follow a $t^2$ dependence, it was still fast because the coalescence of vortices enhanced the plasma mixing, a result also found by *Fujimoto and Terasawa* [1994] and *Fujimoto and Terasawa* [1995]. *Fujimoto and Terasawa* [1995] found that the plasma mixing was reduced, however, for increasing relative density (and relative magnetic field strength) between the magnetosheath and magnetosphere.

Recently, ideal MHD and full-particle simulations carried out by *Matsumoto and Hoshino* [2004] and *Matsumoto and Hoshino* [2006] showed that the KH vortices are rapidly broken down by the growth of secondary KH and Rayleigh Taylor (RT) instabilities within the vortex structure. This break-down causes strong turbulence in the system, and plasma mixing subsequently increases. In our recent hybrid simulation results [*Cowee et al.*, 2009, hereafter referred to as paper 1], we also found this effect to be particularly important in enhancing plasma transport from KHI. Transport by KHI also occurs as a result of reconnection of strongly twisted magnetic fields in KHI vortices even when the IMF is nearly northward [*Nykyri and Otto*, 2001, 2004]; however, as we show later this process does not occur in our simulations.

*Miura* [1995] carried out the first MHD simulations of KHI which included a magnetic shear across the magnetopause. He found that northward IMF (i.e. no magnetic shear) was the most unstable condition, and the growth rate decreased for off-northward angles. For southward IMF the growth rate was positive but the magnetopause only undulated and did not form recognizable KH waves or vortices due to the magnetic tension forces. Since then, more MHD simulations of KHI have included magnetic shear angles within

30° of northward [*Takagi et al.*, 2006; *Keller and Lysak*, 1999], but kinetic simulations have not yet considered this condition.

KH vortices have been identified in spacecraft observations from their particular periodic signatures in flow velocity, magnetic field, density, and temperature. For example, in the *Hasegawa et al.* [2004] report on Cluster observations of the KH-unstable magnetopause during northward IMF conditions, the plasma flow vectors exhibited an anti-clockwise rotation around the vortex center as is expected for the instability at the dusk side of the magnetopause. Correlated with the flow vectors were periodic variations in density and temperature associated with the high density, cold solar wind and the low density, hot magnetospheric plasma. Additionally, both cold solar wind and hot magnetospheric ions were found to co-exist in the same regions on the magnetospheric side of the magnetopause. The magnetic field variations in the high and low density regions were found to have the correct polarity for KH vortices (based on MHD simulations). *Hasegawa et al.* [2004] concluded that this was a rolled-up vortex in which plasma mixing was occurring, but since they did not find the magnetic stresses or D-shaped ion distributions associated with reconnection, they did not believe that process was playing a role in the plasma mixing. Other observations of KH vortices, however, have found evidence for reconnection within the vortices [*Nykyri et al.*, 2006; *Nishino et al.*, 2007].

Rolled-up vortices have also been identified using the single-spacecraft method proposed by *Hasegawa et al.* [2006]. This technique, based on the MHD simulations of *Takagi et al.* [2006], looks for the low density fast tailward flows produced by the vortex motion. Such flows occur within a rolled-up KH vortex because the low density solar wind plasma must rotate faster than the high density magnetospheric plasma so that force balance is

maintained in the radial direction. Using Cluster and Geotail data, *Hasegawa et al.* [2006] showed that the lowest density flows associated with KH vortices had tailward velocities greater than their initial magnetosheath velocities. Similar results from Double Star data were found by *Taylor et al.* [2008] during which evidence for phase space plasma mixing was found in the ion data [*Taylor and Lavraud*, 2008].

Paper 1 describes two-dimensional hybrid simulations of the KHI carried out for conditions with uniform magnetic field across the simulation box (i.e. no magnetic shear across magnetopause) perpendicular to the shear flow velocity (most unstable configuration) with a density jump between the magnetosheath and magnetosphere up to a factor 10. In this manuscript we continue the work described in paper 1 but we include a magnetic shear across the boundary and increase the shear velocity jump, to include more realistic conditions. The paper is organized as follows: section 2 describes the methods used in the paper; section 3 describes the simulation results which include the simulated growth of vortices (section 3.1), what a hypothetical spacecraft would see if it flew through the center of the simulation box (section 3.2), and the diffusion of magnetosheath plasma into the magnetosphere (section 3.3); section 4 summarizes the results.

## 2. Methodology

For our KH-unstable magnetopause configuration, the boundary sits in the middle of the simulation box with the magnetosheath plasma on the left ($-x$) and the magnetosphere plasma on the right ($+x$). The conditions in the magnetosheath ("s") are $n_s = 5$ protons/cc, $B_s = 20$ nT, and $T_{is} = T_{es} = 10$ eV ($\beta = 0.05$, $\rho_L = 23$ km). The conditions in the magnetosphere ("m") are varied depending on the density jump across the magnetopause boundary: equal to 1/4, or 1/10 the density in the magnetosheath. For

uniform density, the magnetosphere conditions are $n_m = 5$ protons/cc, $B_m = 20$ nT, and $T_{im} = T_{em} = 10$ eV ($\beta = 0.05$, $\rho_L = 23$ km). For a density jump of 4, the magnetosphere conditions are $n_m = 1.25$ protons/cc, $B_m = 20$ nT, $T_{im} = T_{em} = 40$ eV ($\beta = 0.05$, $\rho_L = 46$ km). For a density jump of 10, the magnetosphere conditions are $n_m = 0.5$ protons/cc, $B_m = 20$ nT, $T_{im} = T_{em} = 100$ eV ($\beta = 0.05$, $\rho_L = 72$ km). On the magnetosphere side, the magnetic field points northward ($+z$), while on the magnetosheath side, it points at an angle $\theta_s = 0°$, $15°$, or $30°$ away from northward in the $y$-$z$ plane. The velocity shear jump, $V_s$, is equal to 1 $v_A$ calculated on the high density side ($v_A = 195$ km/s), and the shear layer half-thickness, $a$, is 1 $c/\omega_{pi}$ calculated on the high density side ($c/\omega_{pi} = 102$ km). These conditions are meant to be generally representative of the KH-unstable magnetopause conditions and not specifically to any particular spacecraft observations. We start with thin shear layers and let small vortices grow and coalesce in time to larger structures.

In this study we use a two-dimensional hybrid code, the basic equations of which are given in Appendix A. In the calculations we assume a small, constant resistivity ($\eta = 10^{-4}$) and a scalar electron pressure. With such a model, it has been previously shown that magnetic reconnection does not occur unless either a model for the electron pressure tensor [*Hesse et al.*, 1995] or an enhanced localized resistivity [*Kuznetsova et al.*, 1996] is added to break the frozen-in condition in the electric field equation (A8).

The system size is 120 $c/\omega_{pi}$ with 512 grid cells in $x$ direction and 120 $c/\omega_{pi}$ with 512 grid cells in the $y$ direction, where $x$ is normal to the initial magnetopause boundary and $y$ is parallel to it. The boundary conditions are periodic in the $y$ direction and reflective in the $x$ direction. We chose this simulation box size so that multiple wavelengths of the

dominant mode could grow and the interaction can proceed for a long time (i.e., $\Omega_i t \sim 600$) before the reflective boundaries became an issue. All simulations use 100 superparticles per cell and a timestep of $0.05\Omega_i^{-1}$.

## 3. Results and Discussion

### 3.1. Vortex Formation

We carried out a set of nine simulations for each of the combinations of density jump $n_s/n_m = 1$, 4, and 10 and magnetic shear angle $\theta_s = 0°$, 15°, and 30°. Figures 1-3 show the magnetosheath densities in the nine simulations at $\Omega_i t = 150$ and 600. Figure 1, which shows the uniform density simulations, shows that the KHI is unstable for all magnetic shear angles tested, growing from small fluctuations (Figure 1 top panels) to rolled-up vortices which coalesce to eventually form one large vortex structure limited by the simulation box size (Figure 1 bottom panels). The size of the initial vortices are ∼15-20 $c/\omega_{pi}$ consistent with the linear theory prediction that the wavenumber of maximum growth, $k$, is $ka \sim 0.4$ [*Miura and Pritchett*, 1982]. It is interesting that the structure of the large vortex at $\Omega_i t = 600$ for the $\theta_s = 0°$ and $\theta_s = 15°$ simulations appears equally large and rolled-up, yet it is much more coherent in the simulation with the magnetic shear. With an increase in shear angle, the growth rate decreases [*Miura*, 1995], but there is little effect here on the size of the vortex. The reduced growth is evident in the simulation with $\theta_s = 30°$ in that vortex structure is not as large or as rolled-up as in the other simulations. The apparent reduction in short-wavelength turbulence in the $\theta_s = 15°$ and 30° simulations is an interesting effect which will be discussed later.

Figure 2, which shows the $n_s/n_m = 4$ simulations, shows that the KHI is again unstable for all magnetic shear angles tested. The fluctuations begin small and coalesce, but the

vortices are eroded by secondary KH and RT instabilities [*Matsumoto and Hoshino*, 2004], forming long and narrow filamentary structures which can break off and contribute to the turbulent system. At $\theta_s = 0°$, the system is very turbulent at $\Omega_i t = 600$ compared to that at $\theta_s = 15°$ or $\theta_s = 30°$ which show a more coherent KH structure. The structures at $\theta_s = 15°$ and $\theta_s = 30°$ appear more wave-like than vortex-like in comparison to the nicely rolled-up structures in Figure 1, but they do still contain plasma on vortical paths within the structures. The secondary instabilities are active, and are eroding the high-density (magnetosheath plasma) vortex arm as it rolls into the low-density (magnetosphere plasma) region.

Figure 3, which shows the $n_s/n_m = 10$ simulations, shows that the KHI grows for the magnetic shear simulations with $\theta_s = 0°$ and $15°$. At $\theta_s = 30°$, the magnetic tension forces are too high for this non-uniform density simulation to show even a slight undulation of the boundary. We see again that the KH structure at $\Omega_i t = 600$ is more coherent at $\theta_s = 15°$ than $\theta_s = 0°$, and there is much less turbulence present. The KH structure is wave-like as the vortex structure is eroded by secondary instabilities.

An interesting result here is that the simulations with low magnetic shear show a more coherent KH structure at later times than do the simulations for purely northward IMF. In the pure northward case, there is more small-scale turbulence which acts to break-down the vortex structures over time. The effect is particularly enhanced when the density jump between the magnetosheath and magnetosphere is increased because the growth of secondary instabilities is enhanced. With the introduction of magnetic shear there is a magnetic tension force from the nonzero $B_y$ which prevents a more turbulent system from forming. In the non-uniform density simulations, the vortex structure is no longer

rapidly broken down by the turbulence as the growth rates of the secondary instabilities are reduced [*Matsumoto and Hoshino*, 2004]. Small-scale turbulence which disrupts the vortex structure is also seen, as has been found in Hall-MHD simulations of KHI when there is a density jump [*Huba*, 1994; *Nykyri and Otto*, 2004]. Comparison of hybrid and fluid simulations for the Rayleigh-Taylor instability on ion gyroradius scales shows that short wavelength fluctuations are better defined in fluid calculations while particle noise in hybrid calculations tends to obscure small-scale features [*Huba and Winske*, 1998]. To verify that it is the presence of magnetic shear and not just the reduced growth rate of the primary KH-unstable mode which yielded a less turbulent system, we ran simulations with an increased velocity shear up to 2 $v_A$ (not shown). With the larger growth rate from the larger velocity shear, larger vortex structures were generated for the $\theta_s = 15°$ and $\theta_s = 30°$ simulations, but they did not show the turbulent break-down exhibited in the $\theta_s = 0°$ simulations. Additionally, at these higher shear velocities, the $n_s/n_m = 10$ simulation with $\theta_s = 30°$ can generate KH waves (not shown).

### 3.2. Hypothetical Spacecraft Observations

The coherent structure of the nonuniform density simulations with magnetic shear could explain why observations such as those discussed in the Introduction demonstrate clearly periodic structure at the magnetopause which is being attributed to the KHI. If the vortex structure were always rapidly broken down by turbulence then it would be very difficult to identify and would not exhibit a regular periodicity. Figures 4 - 6 show simulated quantities in the grid cells along the $y$ direction in the middle of the simulation box at $\Omega_i t = 150$ for the s with $n_s/n_m = 1$, 4 and 10 with $\theta_s = 15°$. Periodic structure is particularly evident in the uniform density simulation, becoming less regular with the

$n_s/n_m = 4$ simulation, and irregular with the $n_s/n_m = 10$ simulation, though it still exhibits the weak signatures of vortex motion in the fluctuating magnetic field and bulk velocity.

For the uniform density simulations, the periodic structure for the $\theta_s = 0°$ simulation at $\Omega_i t = 150$ (not shown) is very similar to that shown in Figure 4; compared to the $\theta_s = 30°$ simulation at $\Omega_i t = 150$ (not shown), the structure is again regularly periodic, but the velocity and magnetic field perturbations are much smaller in the $x$ direction. For the $n_s/n_m = 4$ simulations, the periodic structure for the $\theta_s = 0°$ simulation at $\Omega_i t = 150$ (not shown) is less regularly periodic than that shown in Figure 5, which is not surprising given the enhanced turbulence in the former simulation. In the $\theta_s = 30°$ simulation at $\Omega_i t = 150$ KHI is not well developed so we consider the simulated quantities at $\Omega_i t = 300$ instead (not shown), which show an irregular periodic structure with weak signatures of vortex motion. For the $n_s/n_m = 10$ simulations, the periodic structure for the $\theta_s = 0°$ simulation at $\Omega_i t = 150$ (not shown) is irregular just as in Figure 6, though signatures of vortex motion can be identified.

The periodic structure exhibits signatures in agreement with the observations, showing alternating periods of high density, low temperature plasma (magnetosheath) and low density, high temperature plasma (magnetosphere) correlated with the perturbations in the magnetic field and bulk plasma flow. From the temperature variations, we see that plasma from the two sides is simply being mixed and is not being heating by the instability.

We also find that the vortices show the low-density fast tailward flows that *Hasegawa et al.* [2006] indicate as a means of identifying rolled-up vortices from single-spacecraft observations. As shown in figure 7, these structures are more defined for $\theta_s = 0°$ (light

gray) than at $\theta_s = 15°$ (dark gray), in agreement with the MHD simulations of *Takagi et al.* [2006]. As the shear angle is increased, the low density flows are not accelerated to as high of tailward velocity as when there is no magnetic shear. Indeed for the $\theta = 30°$ cases, low-density flows faster than the initial shear velocity jump are not generated at all and so are not shown in the figure. Yet the lack of observed low-density, high tailward flows associated with KH vortices [i.e., *Lavraud et al.*, 2009] does not conclusively prove that a vortex is not rolled-up or that plasma mixing is not occurring. Since the flows are formed because of a difference in plasma density across the magnetopause, the uniform density simulations do not generate them even though the vortices are clearly rolled-up (see Figure 1). If the density jump is more than 1 but less than 4 it is also possible that such flows might not be generated, although we have not tested this hypothesis. We note also that these low-density fast tailward flows were obtained in our simulation for vortex structures which rolled up and yielded significant plasma mixing (see next section) through means other than reconnection.

### 3.3. Plasma Transport

To examine plasma transport we calculate the diffusion coefficients in the manner of paper 1. We consider a fundamental treatment of diffusion which involves tracking the particle motion in the direction normal to the magnetopause and then finding the mean square displacement of the particles, $< \Delta x^2 >$, over time. The diffusion coefficient, $S$, is then defined as

$$S =< \Delta x^2 > /t \ . \tag{1}$$

Note that since $B_0$ is northward on the magnetosphere side, the direction perpendicular to the magnetopause boundary is also perpendicular to $B_0$. On the magnetosheath side, diffusion in the plane perpendicular to $B_0$ would involve calculation in a spatial $z$ direction that does not exist in our two-dimensional simulation. We therefore consider $S$ to relate to the direction strictly perpendicular to the magnetopause. For this calculation, we track particles in the region 15 $c/\omega_{pi} < x < 105$ $c/\omega_{pi}$ which includes the interaction region but is away from the reflective boundaries.

Figure 8 shows the calculated mean-square displacement since $\Omega_i t = 0$ and the corresponding diffusion coefficients at several times during the various simulations. As was demonstrated in paper 1, the diffusion coefficients increase in magnitude over time, resembling what [*Treumann*, 1997] referred to as "super-diffusion". This is certainly not diffusion in the classical sense, as the motion of particles and their transport perpendicular to the magnetopause is a function not only of the small-scale turbulence generated by the instabilities but also the large-scale vortex motion. The inseparability of these large and small-scale dynamic effects necessitates that the diffusion coefficient include both. We refer to our diffusion coefficient as $S$ rather than $D$ to avoid misinterpretation of the result as a typical diffusion coefficient that is time-independent.

For the uniform density simulations, the $\theta_s = 15°$ simulation shows a larger $< \Delta x^2 >$ than the $\theta_s = 0°$ simulation because the final vortex in the $\theta_s = 15°$ simulation forms a more coherent large-scale structure; the $\theta_s = 30°$ simulation exhibits a much smaller diffusion coefficient because the size of the instability is reduced. For the non-uniform density simulations, $< \Delta x^2 >$ is largest for $\theta_s = 0°$ where there is the most small-scale turbulence. As the magnetic shear angle is increased $< \Delta x^2 >$ over time is also reduced. In

these simulations, where enhanced turbulence from the secondary instabilities is possible, the more coherent vortex structures for low magnetic shear angles are not as important in enhancing particle transport as the turbulent break-down of the vortices. We note that by $\Omega_i t = 600$, the diffusion coefficients for some of the simulations do appear to be leveling out, which is likely the result of the interaction region in these simulations reaching the edges of the simulation box.

Diffusion coefficients have been estimated in previous hybrid simulation work by *Terasawa et al.* [1992], *Fujimoto and Terasawa* [1994] and *Thomas and Winske* [1993] by finding analytic solutions to an assumed diffusion equation for the system and then solving them using the various derived mixing quantities obtained at late times during the simulation. Because these studies all assumed that diffusion of plasma by KHI is effectively described by a diffusion coefficient which is independent of time, we need to compare their diffusion coefficients with our diffusion coefficients obtained at particular times during the simulations. In the simulations of *Terasawa et al.* [1992] and *Fujimoto and Terasawa* [1994], they each carried out a simulation with velocity shear jump and shear layer half-width similar to ours, however they used a much smaller simulation box. Because the KHI vortices will ultimately grow to fill the simulation box, the box size is fundamental limiting parameter on the plasma transport. In the small-box case, the mixing reaches an asymptotic value over time as the single vortex completely fills the simulation box, is confined by the boundaries, and eventually fully mixes the plasma within the box. Thus we expect their diffusion coefficients to generally agree with ours at times up until the vortices have grown to the size of their simulation boxes. After this time, the vortices in our larger simulation box can continue to grow and we can obtain

larger diffusion coefficients than they did. In the simulations carried out by *Thomas and Winske* [1993], they used a larger simulation box, but considered a smaller velocity shear jump and shear layer half-width than we did. Thus we expect their diffusion coefficients should be smaller than ours, because their instability has a lower growth rate and smaller wavelength KH mode at maximum growth.

*Terasawa et al.* [1992] assumed a constant diffusion coefficient from a fit to the area covered by "mixed" simulation cells (i.e. cells with at least a quarter of their density from each of magnetosheath and magnetosphere particles) over time, and determined $D = 0.21$, 0.33 and $0.49(c/\omega_{pi})^2\Omega_i$ for simulations with $a = 1$, 1.5, and 2 $c/\omega_{pi}$. In terms of comparison to our normalized diffusion coefficients, note that since $a$ is equal to 1 $c/\omega_{pi}$ the values in the Figure 8 can be thought of as normalized to the ion inertial length instead of the velocity shear layer half-width. In this case, the diffusion coefficient from *Terasawa et al.* [1992] for a uniform density simulation with $\theta_s = 0°$, shear layer half-width of 1 $c/\omega_{pi}$ and velocity shear jump of 1 $v_A$ is in agreement with our simulation results obtained around $\Omega_i t = 300$. They obtained their diffusion coefficient from a fit to their simulated mixing at $\Omega_i t > 200$, when the single dominant mode vortex they were simulating had filled the simulation box and the mixing area had reached an asymptotic state. Similarly, *Fujimoto and Terasawa* [1994] used the area of the mixing layer calculated from the number of mixed simulation cells at late times during the simulation run to get a diffusion coefficient of $D = 0.24(c/\omega_{pi})^2\Omega_i$. This value from their uniform density simulation with $\theta_s = 0°$, shear layer half-width of 2 $c/\omega_{pi}$ and shear velocity jump of 1 $v_A$ is also within the range we simulated for times just after $\Omega_i t = 300$.

*Thomas and Winske* [1993] determined diffusion coefficients from the rate of change of the mixing layer width, $\delta Z$, which was a proportional to the number of particles crossing the midplane of the simulation over time. They determined the value of $D$ to be at most $0.03 V_D a$ where $V_D$ is the velocity shear jump ($V_s$ in our simulations). Translated into units normalized by the ion inertial length and gyrofrequency, $D \simeq 0.007(c/\omega_{pi})^2\Omega_i$. This value from their uniform density simulation with $\theta_s = 0°$, shear layer half-width of 0.75 $c/\omega_{pi}$ and velocity shear jump of 0.33 $v_A$ is low compared to our diffusion coefficients probably because of the smaller size and growth rate of the instability and as well as the differences in the techniques employed to compute the diffusion coefficients.

*Fujimoto and Terasawa* [1995] also carried out simulations of KHI growth for a range of non-uniform densities across the magnetopause and velocity shear layer half-widths. They found that the plasma mixing was reduced when the density jump across the magnetopause was increased, in agreement with our results, but they did not calculate diffusion coefficients for the various cases so we cannot provide a comparison.

From these results, we can consider the important issue of whether or not KHI could be a dominant mechanism in the transport of solar wind plasma into the magnetosphere for northward IMF conditions. Because of the magnetospheric magnetic field orientation and the draping of the solar wind magnetic field, reconnection would be expected to be the dominant LLBL population mechanism for conditions except those of northward IMF [*Scholer and Treumann*, 1997]. The canonical diffusivity required for populating the LLBL is $10^9$ m$^2$/s [*Sonnerup*, 1980] which may or may not be achievable through viscous processes on the flanks. The focus has been on plasma waves and drift instabilities driven by density gradients scattering particles in the transition layer, however diffusivities

calculated from only the very highest observed wave amplitudes come close to being large enough [e.g., *Treumann et al.*, 1991; *Vaivads et al.*, 2004].

To compare our normalized simulation results to real-world values, we convert the diffusion coefficients in Figure 8 using shear layer half width $a = 102$ km and gyrofrequency $\Omega_i = 0.3047$ Hz. We calculate that a diffusion coefficient of $10^8$ m$^2$/s is equivalent to $S = 0.03a^2\Omega_i$ (dotted line) and $10^9$ m$^2$/s is equivalent to $S = 0.32a^2\Omega_i$ (dot-dash line). Values greater than $10^9$ m$^2$/s are obtained during the simulations for $n_s/n_m = 1$ with $\theta_s = 0°$ and $\theta_s = 15°$ between $\Omega_i t = 350 - 400$ and the simulation with $n_s/n_m = 4$ with $\theta_s = 0°$ around $\Omega_i t = 450$. This suggests that plasma transport of the order necessary to populate the LLBL could be achieved under certain conditions via KHI; however, we reiterate that our diffusion coefficients are time-dependent and should not be used as if they were classical diffusion coefficients. This result is not without caveats, namely that our system is not a true representation of the global picture. Our simulation is not fully three-dimensional and we do not include truly realistic magnetopause conditions in a large non-periodic-boundary system stretching from nose to tail. Also importantly, our simulation does not model electrons kinetically which is important in truly quantifying the plasma transport and in modeling reconnection on fundamental scales. Additionally, we do not model inhomogeneities in the magnetosphere such as plasma gradients from the plasma sheet and lobes which would ultimately limit the sizes of the vortices. Nevertheless, it is an interesting result that we can generate local, time-dependent diffusion coefficients of the order $10^9$ m$^2$/s in our simple system.

## 4. Summary

We have carried out two-dimensional hybrid simulations (kinetic ions, massless fluid electrons) of the KHI for different density jumps and near-northward magnetic shear angles across the magnetopause, starting with a relatively thin shear layer (∼200 km). For no magnetic shear, the uniform density simulation generates large coherent vortices while in the non-uniform density simulations the coherent vortices are broken down by secondary KH and RT instabilities yielding a more turbulent system. For a magnetic shear angle of $\theta_s = 15°$, the simulations all show a more coherent vortex structure, as the turbulence which previously broke-down the instabilities is reduced. For $\theta_s = 30°$, the magnetic tension force stabilizes the $n_s/n_m = 10$ simulation so it does not generate KH waves, but the $n_s/n_m = 4$ and 1 simulations do. If the shear velocity jump across the magnetopause is increased then the growth rate of the instability increases and a $n_s/n_m = 10$ simulation can generate waves.

Simulation results show periodic structure in density, temperature, bulk velocity and magnetic field in general agreement with spacecraft observations. Periods of low and high density are correlated with period of high and low temperature, as expected for mixing of cold solar wind and hot magnetosphere plasmas in a vortex structure. Also in agreement with observations is the generation of low-density fast tailward flows in the rolled-up vortices for the non-uniform density simulations.

To examine diffusive plasma transport by KHI, we considered the fundamental definition of diffusion and calculated the mean-squared displacement of particles, $< \Delta x^2 >$, over time. Results showed that the $< \Delta x^2 >$ increased nonlinearly with time, and was higher for the uniform density simulations than the non-uniform density simulations and decreased with increasing magnetic shear angle. This non-linear increase in the diffu-

sion coefficient ($S =< \Delta x^2 > /t$) implies enhanced diffusion which is more appropriately considered as "super-diffusion" than classical diffusion [*Cowee et al.*, 2009; *Treumann*, 1997]. It results from the combined effects of large-scale vortex motion and small-scale turbulence generated in the break-down of the vortices.

The efficiency of KHI in transporting magnetosheath plasma into the magnetosphere and populating the LLBL is not well understood, but our results suggest that it could be a more important mechanism than previously thought. The canonical diffusivity required to populate the LLBL is $10^9$ m$^2$/s [*Sonnerup*, 1980]. Transport of this magnitude due to reconnection of twisted fields from the KHI has been measured in the Hall-MHD simulations [*Nykyri and Otto*, 2004] and we find that such diffusivities of this magnitude are obtained in several of our simulations. In the uniform density simulations with $\theta_s = 0°$ and $15°$ and in the $n_s/n_m = 4$ simulation with $\theta_s = 0°$, the time-dependent diffusion coefficient around $\Omega_i t = 400$ (when the smaller vortices that great out of a thin shear layer have coalesced into one or two large vortices in the simulation box) reached values equivalent to $10^9$ m$^2$/s. This result should be treated carefully, since our diffusion coefficients are not classical diffusion coefficients but are instead time-dependent. Additionally, we note that the higher diffusivities yielded by the smaller density jump simulations could suggest that double high-latitude reconnection, which acts to increase the plasma density in the magnetosphere, plays a role in the growth of KHI [*Bouhram et al.*, 2005; *Hasegawa et al.*, 2009] and therefore helps facilitate this enhanced plasma transport.

## Appendix A: Hybrid Model Equations

The two-dimensional hybrid simulation code treats ions kinetically using standard particle-in-cell techniques and treats electrons as a massless, charge neutralizing fluid.

Velocities and electromagnetic fields are maintained in all three directions, while particle position is determined in two dimensions. A leapfrog scheme is used to advance the particle positions and velocities in time.

The particle motion is described by the equations of motion:

$$m_i \frac{d\mathbf{v_p}}{dt} = q_i(\mathbf{E} + \frac{\mathbf{v_p} \times \mathbf{B}}{c}) - e\eta\mathbf{J}, \tag{A1}$$

$$\frac{d\mathbf{x_p}}{dt} = \mathbf{v_p}, \tag{A2}$$

where $m_i$ is the ion species mass, $q_i$ is the ion species charge, $\mathbf{v_p}$ is the particle's velocity, $\mathbf{x_p}$ is the particle's position. The term $e\eta\mathbf{J}$ is a resistivity term where $e$ is the proton charge, $\eta$ is the resistivity, and $\mathbf{J}$ is the current. The electromagnetic fields $\mathbf{E}$ and $\mathbf{B}$ are determined on the spatial grid and interpolated to the position of the particle. From this the ion species number density ($n_i$), charge density ($q_i n_i$), flow velocity ($\mathbf{V_i}$), and current ($\mathbf{J_i}$) can also be specified on the grid for each species and then collected for all species to determine the total ion density and current.

Electrons are treated as a massless fluid ($m_e = 0$) so the electron momentum equation becomes

$$n_e m_e \frac{d\mathbf{V_e}}{dt} = 0 = -en_e(\mathbf{E} + \frac{\mathbf{V_e} \times \mathbf{B}}{c}) - \nabla \cdot \mathbb{P} + en_e\mathbb{R} \cdot \mathbf{J}, \tag{A3}$$

where $-e$ is the electron charge, $n_e$ is the electron number density, $\mathbf{V_e}$ is the electron fluid velocity, $\mathbb{P}$ is the electron pressure tensor, and $\mathbb{R}$ is the resistivity. The plasma is considered as quasi-neutral, such that

$$en_e = q_i n_i. \tag{A4}$$

Electromagnetic fields are solved in the low frequency approximation. With the quasi-neutrality condition, Ampere's law becomes

$$\nabla \times \mathbf{B} = \frac{4\pi}{c}\mathbf{J} = \frac{4\pi}{c} q_i n_i (\mathbf{V_i} - \mathbf{V_e}), \tag{A5}$$

where $\mathbf{V_i}$ is the ion velocity, and Faraday's law is

$$\frac{\partial \mathbf{B}}{\partial t} = -c(\nabla \times \mathbf{E}), \tag{A6}$$

and also

$$\nabla \cdot \mathbf{B} = 0. \tag{A7}$$

Substitution of A5 into A3 removes $\mathbf{V_e}$ and thus gives the equation for the electric field as

$$\mathbf{E} = -\frac{\mathbf{V_i} \times \mathbf{B}}{c} - \frac{(\nabla \times \mathbf{B}) \times \mathbf{B}}{4\pi n_e e c} - \frac{\nabla \cdot \mathbb{P}}{e n_e} + \mathbb{R} \cdot \mathbf{J}. \tag{A8}$$

Usually $\mathbb{P}$ is taken to be a scalar, $\mathbb{P} = p_e \mathbf{1}$, with $p_e = n_e T_e$ and an adiabatic law is assumed for the electron temperature $T_e$. $\mathbb{R}$ is also usually taken as a scalar, $\mathbb{R} = \eta \mathbf{1}$. $\mathbf{E}$ is then only a function of $\mathbf{B}$, $\mathbf{V_i}$, and $n_e$. $\mathbf{B}$ is advanced with a 4th order Runge-Kutta scheme using a smaller timestep than that for the particle push. Given $\mathbf{B}$ and $n_e$ advanced to the next time level, $\mathbf{E}$ can be directly evaluated at the next time level if $\mathbf{V_i}$ is known at that time. Finding the $\mathbf{V_i}$ at the new time is the key feature of all hybrid algorithms [see *Winske et al.*, 2003, for details]. We use a simple Richardson extrapolation to get $\mathbf{V_i}$ from its previously two saved values.

**Acknowledgments.** The authors thank Benoit Lavraud for helpful discussions and support on this project. This work was performed under the auspices of the U.S. Department of Energy (DOE). It was supported by the Living with a Star TR&T and the

Solar and Heliospheric Physics SR&T Programs of the National Aeronautics and Space Administration.

## References

Axford, W. I. (1964), Viscous interaction between the solar wind and the Earth's magnetosphere, *Planet. Space Sci.*, *12*, 45–53.

Bouhram, M., B. Klecker, G. Paschmann, s. Haaland, H. Hasegawa, A. Blagau, H. Reme, J.-A. Sauvaud, L. M. Kistler, and A. Balogh (2005), Survey of energetic O+ ions near the dayside mid-latitude magnetopause with Cluster, *Ann. Geophys.*, *23*, 1281–1294.

Chen, S., M. G. Kivelson, J. Gosling, R. J. Walker, and A. J. Lazarus (1993), Anomalous aspects of magnetosheath flow and of the shape and oscillations of the magnetopause during an interval of strongly northward interplanetary magnetic field, *J. Geophys. Res.*, *98*(A4), 5727–5742.

Cowee, M. M., D. Winske, and S. P. Gary (2009), Two-dimensional hybrid simulations of superdiffusion at the magnetopause driven by Kelvin-Helmholtz instability, *J. Geophys. Res.*, *114*, A10209, doi:10.1029/2009JA014222.

Fairfield, D., A. Otto, T. Mukai, S. Kokubun, R. Lepping, J. Steinberg, A. J. Lazarus, and T. Yamamoto (2000), Geotail observations of the Kelvin-Helmholtz instability at the equatorial magnetotail boundary for parallel northward fields, *J. Geophys. Res.*, *105*(A9), 21,159–21,173.

Fujimoto, M., and T. Terasawa (1994), Anomalous ion mixing with an MHD scale Kelvin-Helmholtz vortex, *J. Geophys. Res.*, *99*(A5), 8601–8613.

Fujimoto, M., and T. Terasawa (1995), Anomaous ion mixing within an MHD scale Kelvin-Helmholtz vortex. 2. Effects of inhomogeneity, *J. Geophys. Res.*, *100*(A7), 12,025–12,033.

Hasegawa, H., M. Fujimoto, T. Phan, H. Reme, A. Balogh, M. Dunlop, C. Hashimoto, and R. Tandokoro (2004), Transport of solar wind into Earth's magnetosphere through rolled-up Kelvin-Helmholtz vortices, *Nature*, *430*(7001), 755–758.

Hasegawa, H., M. Fujimoto, K. Takagi, Y. Saito, and T. Mukai (2006), Single-spacecraft detection of rolled-up Kelvin-Helmholtz vortices at the flank magnetopause, *J. Geophys. Res.*, *111*(A9), A09203, doi:10.1029/2006JA011728.

Hasegawa, H., A. Retino, A. Vaivads, Y. Khotyaintsev, M. Andre, T. K. M. Nakamura, W.-L. Teh, B. U. O. Sonnerup, S. J. Schwartz, Y. Seki, M. Fujimoto, Y. Saito, H. Reme, and P. Canu (2009), Kelvin-Helmholtz waves at the Earth's magnetopause: Multiscale development and associated reconnection, *J. Geophys. Res.*, *114*, A12207, doi:10.1029/2009JA014042.

Hesse, M., D. Winske, and M. M. Kuznetsova (1995), Hybrid modeling of collisionless reconnection in two-dimensional current sheets: Simulations, *J. Geophys. Res.*, *100*(A11), 21,815–21,825.

Huba, J. D. (1994), Hall dynamics of the Kelvin-Helmholtz instability, *Phys. Rev. Lett.*, *72*(13), 2033–2036.

Huba, J. D., and D. Winske (1998), Rayleigh-Taylor instability: Comparison of hybrid and nonideal magnetohydrodynamic simulations, *Phys. Plasmas*, *5*(6), 2305–2316.

Imber, S. M., S. E. Milan, and B. Hubert (2007), Observations of significant flux closure by dual lobe reconnection, *Ann. Geophys.*, *25*, 1617–1627.

Keller, K. A., and R. L. Lysak (1999), A two-dimensional simulation of the Kelvin-Helmholtz instability with magnetic shear, *J. Geophys. Res.*, *104*(A11), 25,097–25,103.

Kuznetsova, M. M., M. Hesse, and D. Winske (1996), Ion dynamics in a hybrid simulation of magnetotail reconnection, *J. Geophys. Res.*, *101*(A12), 27,351–73.

Lavraud, B., M. F. Thomsen, B. Lefebvre, S. J. Schwartz, K. Seki, T. D. Phan, Y. L. Wang, A. Fazakerley, H. Reme, and A. Balogh (2006), Evidence for newly closed magnetosheath field lines at the dayside magnetopause under northward IMF, *J. Geophys. Res.*, *111*, A05211, doi:10.1029/2005JA011266.

Lavraud, B., J. E. Borovsky, V. Genot, S. J. Schwartz, J. Birn, A. N. Fazakerley, M. W. Dunlop, M. G. G. T. Taylor, H. Hasegawa, A. P. Rouillard, J. Berchem, Y. Bogdanova, D. Constantinescu, I. Dandouras, J. P. Eastwood, C. Escoubet, H. Frey, C. Jacquey, E. Panov, Z. Y. Pu, C. Shen, J. Shi, D. G. Sibeck, M. Volwerk, and J. A. Wild (2009), Tracing solar wind plasma entry into the magnetosphere using ion-to-electron temperature ratio, *Geophys. Res. Lett.*, *36*, L18109, doi:10.1029/2009GL039442.

Marcucci, M. F., I. Coco, D. Ambrosino, E. Amata, S. E. Milan, M. B. Bavassano Cattaneo, and A. Retino (2008), Extended SuperDARN and IMAGE observations for northward IMF: Evidence for dual lobe reconnection, *J. Geophys. Res.*, *113*, A02204, doi:10.1029/2007JA012466.

Matsumoto, Y., and M. Hoshino (2004), Onset of turbulence induced by a Kelvin-Helmholtz vortex, *Geophys. Res. Lett.*, *31*, L07303, doi:10.1029/2003GL018970.

Matsumoto, Y., and M. Hoshino (2006), Turbulent mixing and transport of collisionless plasmas across a stratified velocity shear layer, *J. Geophys. Res.*, *111*(A5), A10206, doi:10.1029/2006JA011762.

513 Min, K. W., T. Kim, and H. Lee (1997), Effects of magnetic reconnection in the Kelvin-
514 Helmholtz instability at the magnetospheric boundary, *Planet. Space Sci.*, *45*(4), 495–
515 510.

516 Miura, A. (1995), Dependence of the magnetopause Kelvin-Helmholtz instability on the
517 orientation of the magnetosheath magnetic field, *Geophys. Res. Lett.*, *22*(21), 2993–
518 2996.

519 Miura, A., and P. Pritchett (1982), Nonlocal stability analysis of the MHD Kelvin-
520 Helmholtz instability in a compressible plasma, *J. Geophys. Res.*, *87*(A9), 7431–7444.

521 Nakamura, T., and M. Fujimoto (2005), Magnetic reconnection within rolled-up MHD-
522 scale Kelvin-Helmholtz vortices: Two-fluid simulations including finite electron inertial
523 effects, *Geophys. Res. Lett.*, *32*, L21102, doi:10.1029/2005GL023362.

524 Nishino, M. N., M. Fujimoto, G. Ueno, T. Mukai, and S. Y. (2007), Origin of temperature
525 anisotropies in the cold plasma sheet: Geotail observations around the Kelvin-Helmholtz
526 vortices, *Ann. Geophys.*, *25*, 2068–2086.

527 Nykyri, K., and A. Otto (2001), Plasma transport at the magnetospheric boundary due
528 to reconnection in Kelvin-Helmholtz vortices, *Geophys. Res. Lett.*, *28*(18), 3565–3568.

529 Nykyri, K., and A. Otto (2004), Influence of the Hall term on KH instability and recon-
530 nection inside KH vortices, *Ann. Geophys.*, *22*(3), 935–949.

531 Nykyri, K., A. Otto, B. Lavraud, C. Mouikis, L. Kistler, A. Balogh, and H. Reme (2006),
532 Cluster observations of reconnection due to the Kelvin-Helmholtz instability at the
533 dawnside magnetospheric flank, *Ann. Geophys.*, *24*, 2619–2643.

534 Ogilvie, K. W., and R. J. Fitzenreiter (1989), The Kelvin-Helmholtz instability at the
535 magnetopause and inner boundary layer surface, *J Geophys Res*, *94*(A11), 15,113–

15,123.

Phan, T., C. Escoubet, L. Rezeau, R. Treumann, A. Vaivads, G. Paschmann, S. A. Fuselier, D. Attie, B. Rogers, and B. Sonnerup (2005), Magnetopause Processes, *Space. Sci. Rev.*, *118*, 367–424.

Scholer, M., and R. Treumann (1997), The low-latitude boundary layer at the flanks of the magnetosphere, *Space Sci. Rev.*, *80*, 341–367.

Sonnerup, B. (1980), Theory of the low-latitude boundary layer, *J. Geophys. Res.*, *85*, 2017–2026.

Takagi, K., C. Hashimoto, H. Hasegawa, M. Fujimoto, and R. Tandokoro (2006), Kelvin-Helmholtz instability in a magnetotail flank-like geometry: three-dimensional MHD simulations, *J. Geophys. Res.*, *111*(A8), A08202, doi:10.1029/2006JA011631.

Taylor, M., and B. Lavraud (2008), Observation of three distinct ion populations at the Kelvin-Helmholtz-unstable magnetopause, *Ann. Geophys.*, *26*(6), 1559–1566.

Taylor, M., B. Lavraud, C. Escoubet, S. Milan, K. Nykyri, M. Dunlop, J. Davies, R. Friedel, H. Frey, Y. Bogdanova, A. Asnes, H. Laakso, P. Travincek, A. Masson, and H. Opgenoorth (2008), The plasma sheet and boundary layers under northward IMF: A multi-point and multi-instrument perspective, *Adv. Space Res.*, *41*(10), 1619–1629.

Terasawa, T., M. Fujimoto, H. Karimabadi, and N. Omidi (1992), Anomalous ion mixing within a Kelvin-Helmholtz vortex in a collisionless plasma, *Phys. Rev. Lett.*, *68*(18), 2778–2781.

Thomas, V., and D. Winske (1993), Kinetic simulations of the Kelvin-Helmholtz instability, *J. Geophys. Res.*, *98*(A7), 11,425–11,438.

Treumann, R. (1997), Theory of super-diffusion for the magnetopause, *Geophys. Res. Lett.*, *24*(14), 1727–1730.

Treumann, R., J. LaBelle, and T. M. Bauer (1991), Plasma diffusion at the magnetopause: the case of lower hybrid drift waves, *J. Geophys. Res.*, *96*(A9), 16,009–13.

Vaivads, A., M. Andre, S. C. Buchert, J. E. Wahlund, A. N. Fazakerley, and N. Cornilleau-Wehrlin (2004), Cluster observations of lower hybrid turbulence within thin layers at the magnetopause, *Geophys. Res. Lett.*, *31*, L03804, doi:10.1029/2003GL018142.

Winske, D., L. Yin, N. Omidi, H. Karimabadi, and K. Quest (2003), Hybrid codes: Past, present, future - A tutorial, in *Lecture Notes in Physics v. 615*, pp. 136–265, Springer, Berlin.

**Figure 1.** Magnetosheath density at two times during the simulations with $n_s/n_m = 1$ for $\theta_s = 0°$ (left), 15° (middle) and 30° (right).

**Figure 2.** Magnetosheath density at two times during the simulations with $n_s/n_m = 4$ for $\theta_s = 0°$ (left), 15° (middle) and 30° (right).

**Figure 3.** Magnetosheath density at two times during the simulations with $n_s/n_m = 10$ for $\theta_s = 0°$ (left), 15° (middle) and 30° (right).

**Figure 4.** Simulated quantities in the grid cells along the $y$ direction at $x = 60c/\omega_{pi}$ at $\Omega_i t = 150$ for the simulation with $n_s/n_m = 1$ and $\theta_s = 15°$. Shown are the density, parallel temperature, $v(x, y)$ vectors, $B(x, y)$ vectors, and $B_z$.

**Figure 5.** Simulated quantities in the grid cells along the $y$ direction at $\Omega_i t = 150$ for the simulation with $n_s/n_m = 4$ and $\theta_s = 15°$. Shown are the density, parallel temperature, $v(x, y)$ vectors, $B(x, y)$ vectors, and $B_z$.

**Figure 6.** Simulated quantities in the grid cells along the $y$ direction at $\Omega_i t = 150$ for the simulation with $n_s/n_m = 10$ and $\theta_s = 15°$. Shown are the density, parallel temperature, $v(x, y)$ vectors, $B(x, y)$ vectors, and $B_z$.

**Figure 7.** Simulated bulk $v_y$ versus density at $\Omega_i t = 300$ for the simulations with $n_s/n_m = 4$ (top) and $n_s/n_m = 10$ (bottom) for $\theta_s = 0°$ (light gray) and $\theta_s = 15°$ (dark gray).

**Figure 8.** (Left) Mean-square displacement and (right) diffusion coefficients for the various simulations. Diffusion coefficients equivalent to $10^8$ m$^2$/s and $10^9$ m$^2$/s are indicated by the dotted and dot-dash lines, respectively.

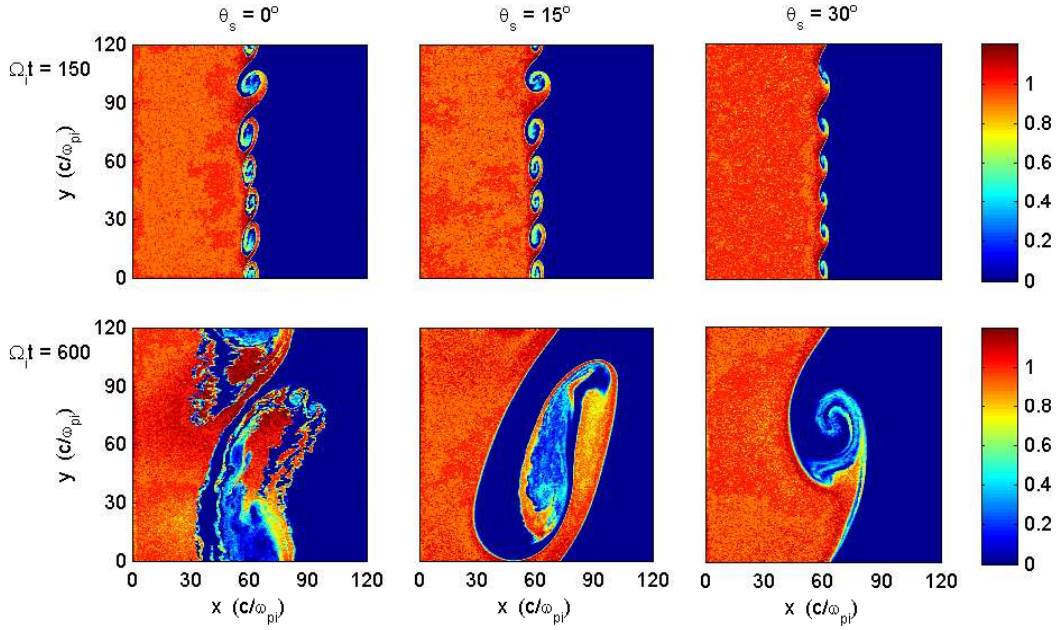


**Figure 1.** Magnetosheath density at two times during the simulations with $n_s/n_m = 1$ for $\theta_s = 0°$ (left), 15° (middle) and 30° (right).

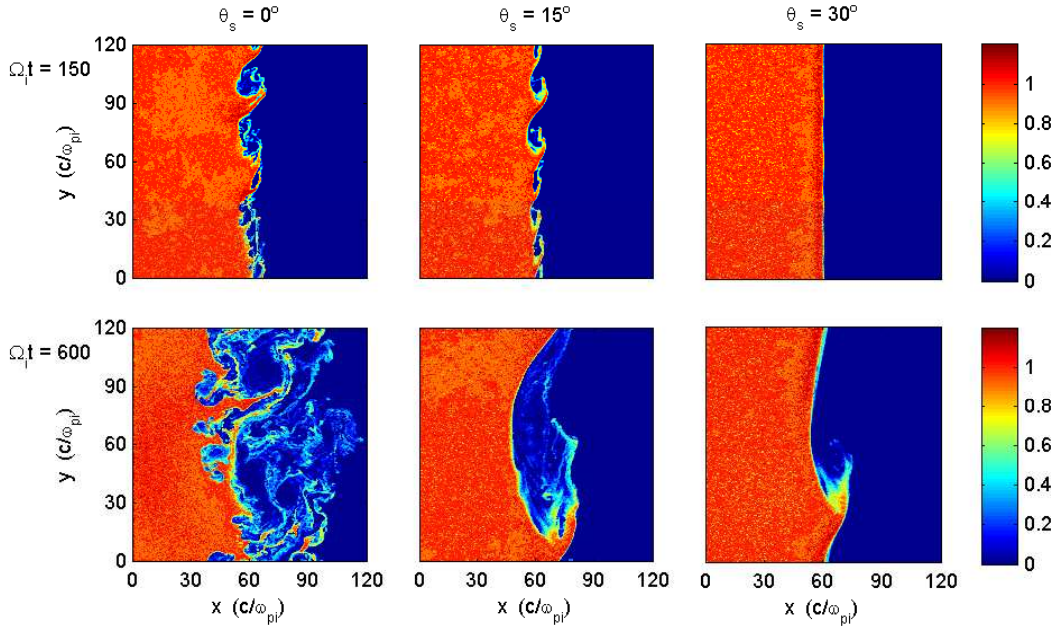


**Figure 2.** Magnetosheath density at two times during the simulations with $n_s/n_m = 4$ for $\theta_s = 0°$ (left), 15° (middle) and 30° (right).

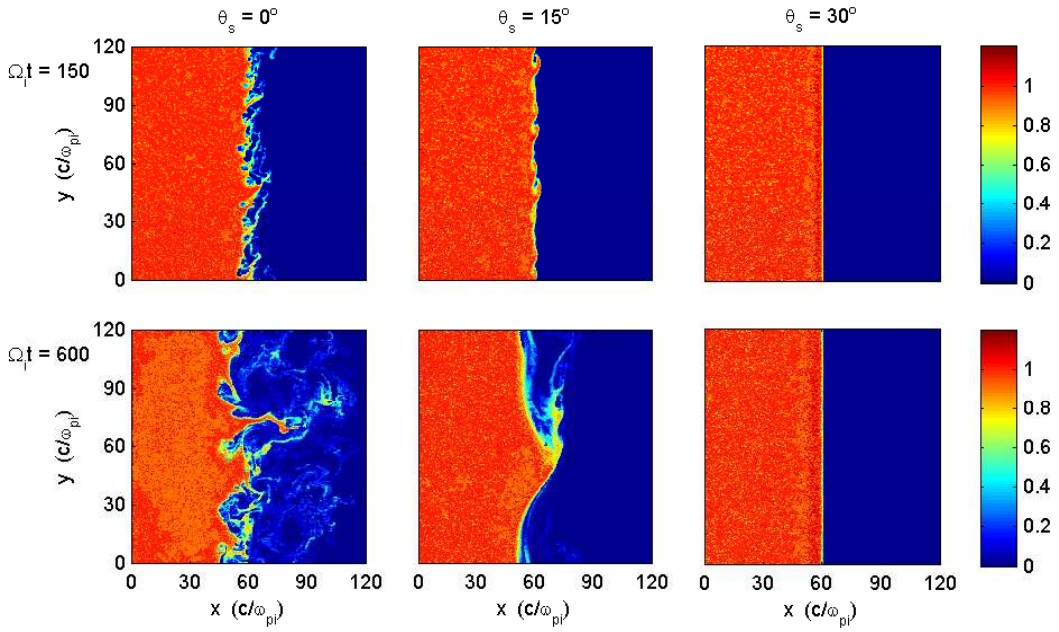


**Figure 3.** Magnetosheath density at two times during the simulations with $n_s/n_m = 10$ for $\theta_s = 0°$ (left), 15° (middle) and 30° (right).

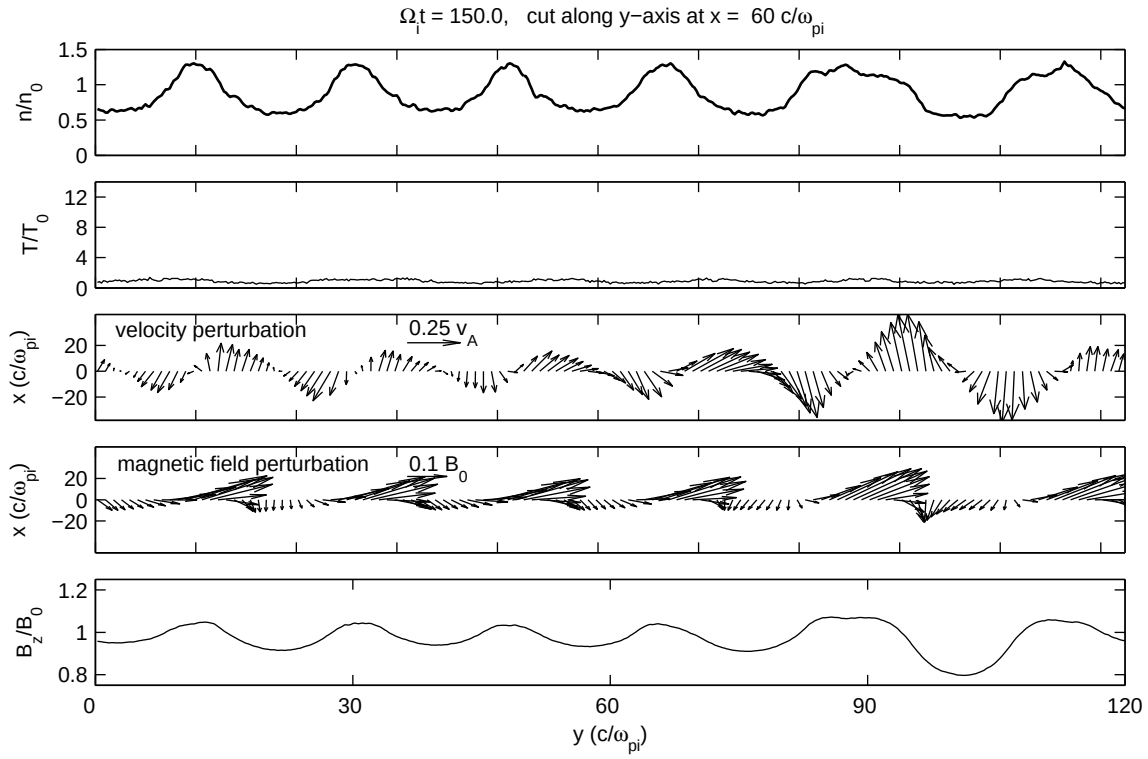


**Figure 4.** Simulated quantities in the grid cells along the $y$ direction at $x = 60c/\omega_{pi}$ at $\Omega_i t = 150$ for the simulation with $n_s/n_m = 1$ and $\theta_s = 15°$. Shown are the density, parallel temperature, $v(x, y)$ vectors, $B(x, y)$ vectors, and $B_z$.

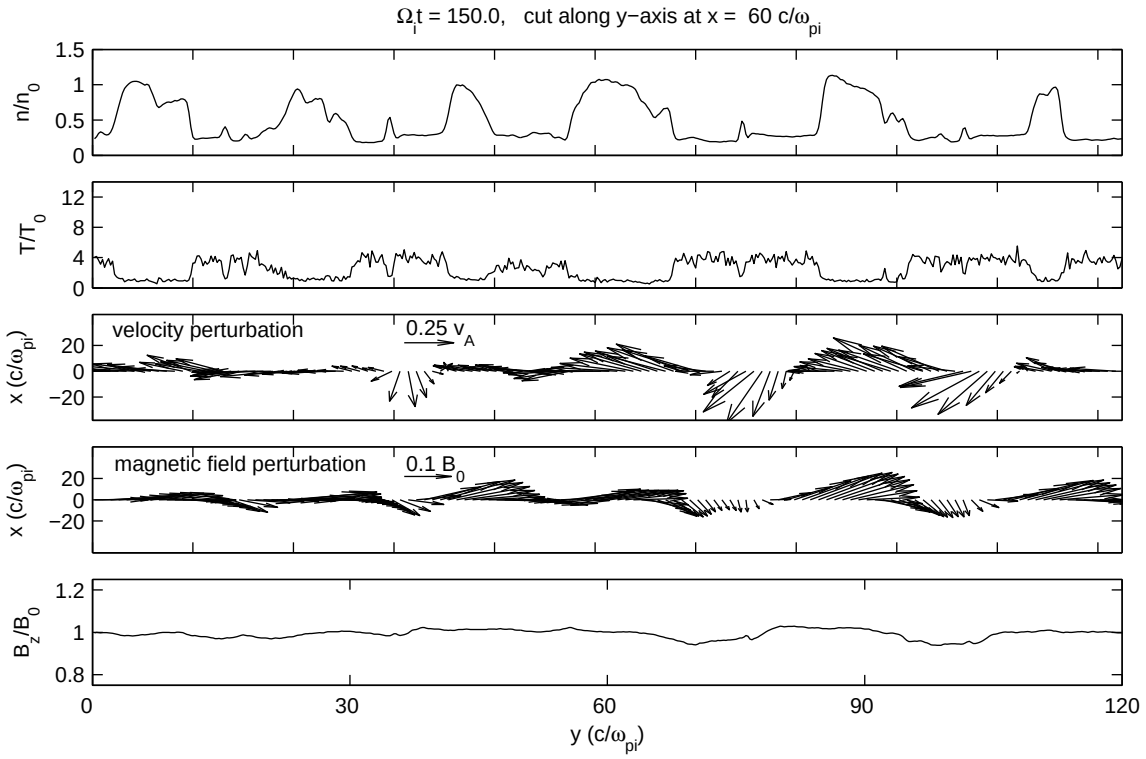


**Figure 5.** Simulated quantities in the grid cells along the $y$ direction at $\Omega_i t = 150$ for the simulation with $n_s/n_m = 4$ and $\theta_s = 15°$. Shown are the density, parallel temperature, $v(x, y)$ vectors, $B(x, y)$ vectors, and $B_z$.

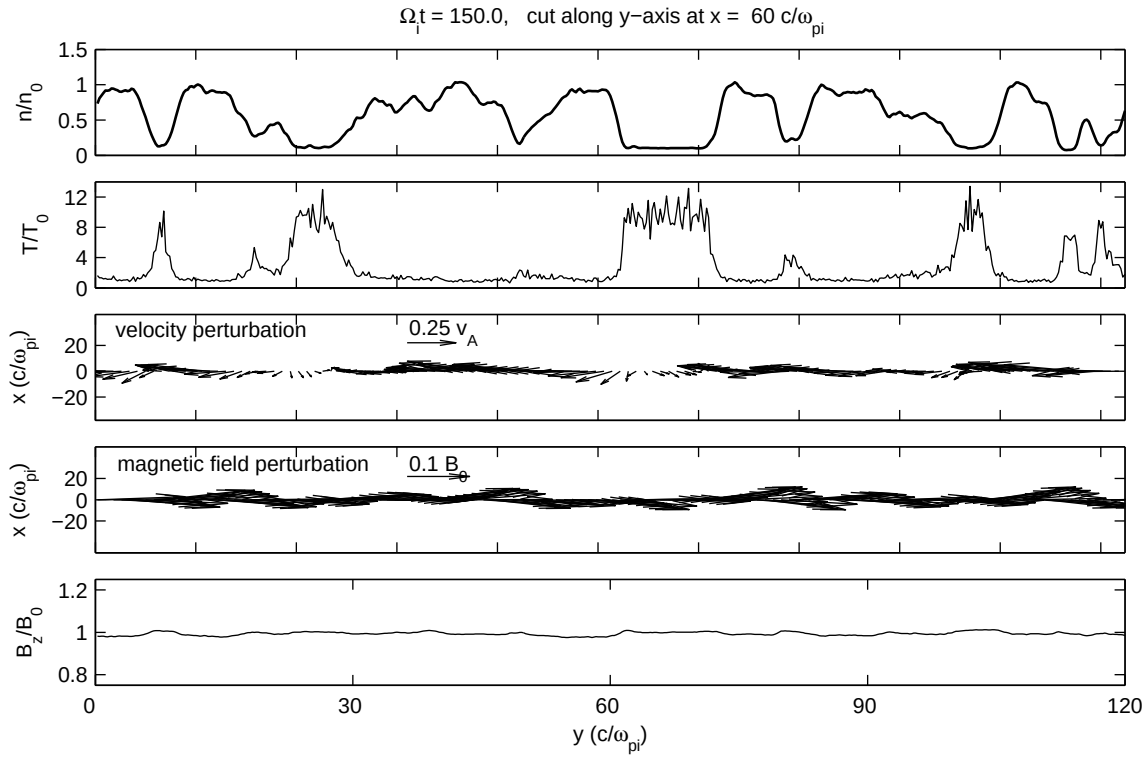


**Figure 6.** Simulated quantities in the grid cells along the $y$ direction at $\Omega_i t = 150$ for the simulation with $n_s/n_m = 10$ and $\theta_s = 15°$. Shown are the density, parallel temperature, $v(x, y)$ vectors, $B(x, y)$ vectors, and $B_z$.

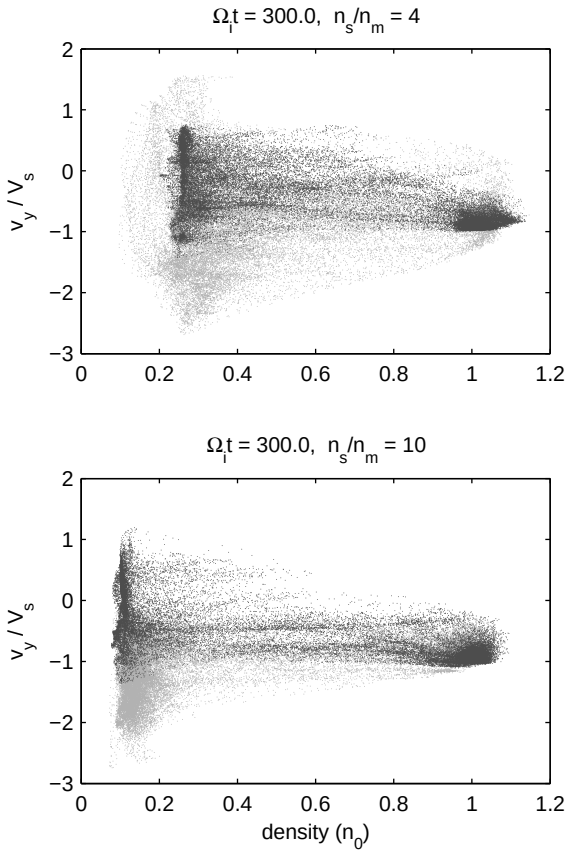


**Figure 7.** Simulated bulk $v_y$ versus density at $\Omega_i t = 300$ for the simulations with $n_s/n_m = 4$ (top) and $n_s/n_m = 10$ (bottom) for $\theta_s = 0°$ (light gray) and $\theta_s = 15°$ (dark gray).

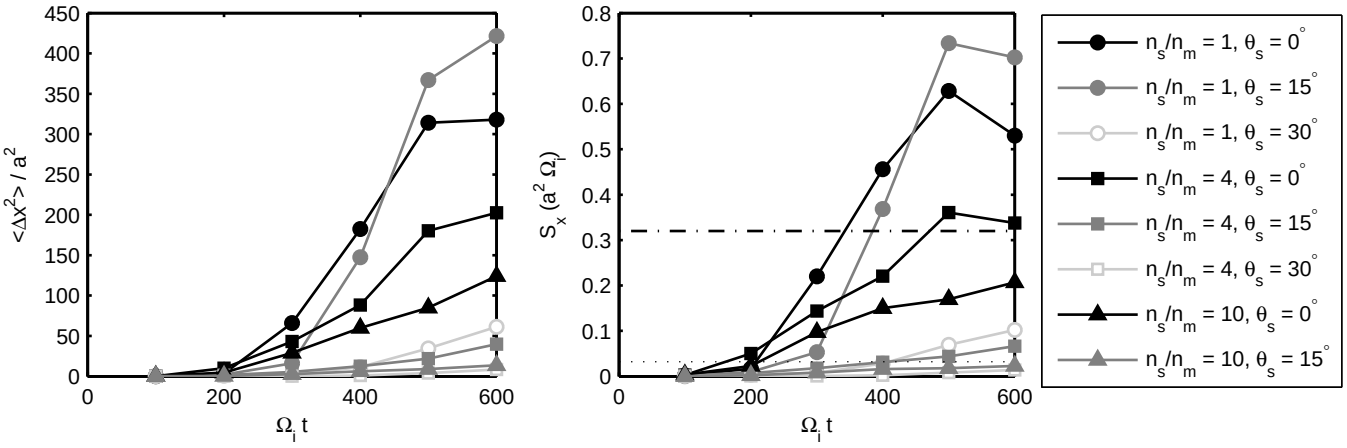


**Figure 8.** (Left) Mean-square displacement and (right) diffusion coefficients for the various simulations. Diffusion coefficients equivalent to $10^8$ m$^2$/s and $10^9$ m$^2$/s are indicated by the dotted and dot-dash lines, respectively.